Separation of transport in slow and fast time-scales using modulated heat pulse experiments (hysteresis in flux explained)

M. van Berkel[1], G. Vandersteen[2], H.J. Zwart[3*,4], G.M.D. Hogeweij[1], J. Citrin[1], E. Westerhof[1], D. Peumans[2], M.R. de Baar[1,3]

[1]DIFFER-Dutch Institute for Fundamental Energy Research, PO Box 6336, 5600 HH Eindhoven, The Netherlands
[2]Vrije Universiteit Brussel (VUB), Dept. of Fundamental Electricity and Instrumentation, Pleinlaan 2, 1050 Brussels, Belgium
[3]Eindhoven University of Technology, Dept. of Mechanical Engineering, Control Systems Technology group (*D&C group), PO Box 513, 5600 MB Eindhoven, The Netherlands
[4]University of Twente, Dept. of Applied Mathematics, PO Box 217, 7500AE, Enschede, The Netherlands

Abstract. Old and recent experiments show that there is a direct response to the heating power of transport observed in modulated ECH experiments both in tokamaks and stellarators. This is most apparent for modulated experiments in the Large Helical Device (LHD) and in Wendelstein 7 advanced stellarator (W7-AS). In this paper we show that: 1) This power dependence can be reproduced by linear models and as such hysteresis (in flux) has no relationship to hysteresis as defined in the literature; 2) Observations of "hysteresis" (in flux) and a direct response to power can be perfectly reproduced by introducing an error in the estimated deposition profile as long as the errors redistribute the heat over a large radius; 3) Non-local models depending directly on the heating power can also explain the experimentally observed Lissajous curves (hysteresis); 4) How non-locality and deposition errors can be recognized in experiments and how they affect estimates of transport coefficients; 5) From a linear perturbation transport experiment, it is not possible to discern deposition errors from non-local fast transport components (mathematically equivalent). However, when studied over different operating points non-linear-non-local transport models can be derived which should be distinguishable from errors in deposition profile. To show all this, transport needs to be analyzed by separating the transport in a slow (diffusive) time-scale and a fast (heating/non-local) time-scale, which can only be done in the presence of perturbations.

Submitted to: *Nucl. Fusion*

1. Introduction

Experiments in 1988 at the tokamak de Fontenay-aux-Roses (TFR) performed by the FOM ECRH team showed that electron transport in fusion plasmas can have a fast response to applied heating power [1], which is much faster than the settling of the temperature profiles. This important observation has been extensively studied and is known as ballistic transport [2]. In Wendelstein 7 advanced stellarator (W7-AS), this led to the concept of hysteresis in the gradient heat flux relationship ($q_e - \nabla_\rho T_e$) originally introduced in the 1990's by Stroth et al. [3]. The importance of studying this concept in detail is shown in [4, 5] where the degradation of confinement with power are directly related through the power dependence of the diffusion coefficient. Moreover, this observation seems to be directly linked to many so-called non-local observations such as the concept of missing power and the fast response of the plasma observed when applying several cold pulse techniques [6]. Although recent simulations suggests that it can also be explained by local transport mechanisms [7]. Based on these studies, the concept of hysteresis could be partially coupled to observations in tokamaks [5, 8].

In this decade (10's) important new experiments and analysis performed in the large helical device (LHD) have renewed the interest in the dependence of transport on power by directly calculating the time evolution of the heat flux against the spatial temperature gradient for a block-wave modulation assuming a standard heat equation. This showed a Lissajous curve which resembles a hysteresis-like time evolution [9].

Recently (2016), experiments at LHD performed in the same regime as the previous discussed phenomena showed that the response to a ECH perturbation is nearly linear [10], where linearity means that the superposition property (additive and homogeneity) is fulfilled. The result in [10] is consistent with previous results at W7-AS and other machines [11, 12]. This seriously questions the conclusions that the phenomenon is hysteresis, which is a strongly non-linear phenomenon [9]. Therefore, in this paper we will show that the observed hysteresis-like behavior is not actual hysteresis but is either the result of an error between the deposition profile used to calculate the heat flux and the actual deposition profile or the result of a projection in the $q_e - \nabla_\rho T_e$ plane of a two-dimensional dependence of the heat flux on both $\nabla_\rho T_e$ and the modulated input power as was implied by [5]. The observed phenomena can also be a combination of both. This fits perfectly with the linearity of perturbative experiments as observed in many experiments [12].

The power dependency of the diffusion coefficient [5] and corresponding Lissajous curves is one possible approach to address the fast transport. There are also other possible extensions which have been suggested in the literature to incorporate this fast transport. One example is by making the diffusion coefficient time dependent [13]. Interestingly, its linearization results in a similar power dependence as derived here [5]. Moreover, there are other approaches in which the models are adjusted such that they can incorporate a non-local diffusivity, e.g., through a fractional diffusion model [14, 15] and using a two-field critical gradient model that couples a heat equation to an evolution equation for the turbulence intensity [16]. We will not analyze these models as we try to build a heat flux model based on experimental observations.

Based on the linearity observation, the heat flux model is reformulated showing that the heat flux contribution is directly related to fast transport mechanisms (non-locality). These are mechanisms which transport heat on a time-scale much faster than the diffusive time-scale, i.e., on the time-scale of the power modulation less than 1 ms.

There are strong indications that turbulence is the dominant physical mechanism driving this fast transport [5, 9, 17], especially since a similar Lissajous curve is observed in the measurements of micro-density fluctuations [9]. However, based on the here discussed perturbative experiments only, it is not possible to distinguish between the different physical mechanisms which drive the fast transport. Moreover, errors in the deposition profile are mathematically indistinguishable from the fast transport components when only analyzing the temperature. Hence, we will not discuss them in detail in this paper. Instead, we will show how the power dependence of the combined fast mechanisms and deposition errors can be extracted from the heat flux allowing to build transport models which capture this fast transport component. To do this, heat flux dependence on fast transport will be rewritten in terms of a mapping from deposition profiles. As this mapping should be independent of the perturbation and deposition profile used, it offers

a path to quantify and predict the combined fast transport and deposition errors in the future. As the fast transport effectively acts as a redistribution of power as has been observed in [18, 19, 2], it also reduces the spatial decay of the amplitude and phase profiles and consequently biases the estimates of transport coefficients.

The goal of this paper is not to describe specific transport mechanisms but to develop a model structure in which the possibly different (physics) mechanisms can be captured and distinguished. Finally, as the term hysteresis is not appropriate to describe the heat flux dependence on power, we will use the term Lissajous curve to describe the observations in the $q - \nabla_\rho T_e$ plane, even though the term Lissajous curve is not entirely correct as it is a term reserved for sinusoidal modulations [20].

This paper is organized as follows. Sec. 2 introduces the basic concepts such as the transport model (heat equation), the estimation procedure of the heat flux, and shows why perturbative experiments are generally linear. Sec. 3 presents simulations and analytical calculations to show that it is not possible to have the observed Lissajous curves on total power errors, but a wide broadening of the deposition profile is necessary. Sec. 4 discusses, analyzes, and extends the different models to describe the (non-local) power dependency of the heat flux in W7-AS and LHD. These set the basis for a combined transport model reached in Sec. 5. Showing that some transport contributions can be discerned. Moreover, this section discusses several mechanisms that can explain the observations in the literature. Finally, the results are briefly summarized and discussed.

2. Heat flux reconstruction using perturbative heat pulse experiments

In this section is explained how the (perturbative) heat flux is attained from perturbative measurements using the heat equation. Moreover, we will show that the perturbations used in the experiments to observe the so-called "hysteresis in flux" can be considered linear. This will be used in the next section to reproduce the so-called "hysteresis in flux", which we will refer to as Lissajous curves a term also used in the caption in [9, Fig. 5].

2.1. Direct calculation of the heat flux

In most transport studies the heat equation (first law of thermodynamics) is used to study (electron) transport in both tokamaks and stellarators [12], i.e.,

$$\frac{\partial}{\partial t}\left(n_e T_e\left(\rho,t\right)\right) = \nabla_\rho\left(-q_e\left(\rho,t\right)\right) + P\left(\rho,t\right), \qquad (1)$$

where $T_e\left(\rho,t\right)$ is the (electron) temperature, ρ the (dimensionless) spatial coordinate, n_e the (electron) density, and $P\left(\rho,t\right)$ the heating power density, which depends on both the time and the radial distribution. The heat equation (1) defines the heat flux we study in experiments. Therefore, in [21] and [9], it is proposed to calculate directly the heat flux q_e by re-expressing the heat equation (1) in terms of q_e. The difference between the approach proposed in [21] and [9] is that in [21] all different power contributions are taken into account whereas [9] tries to take only the perturbative component into account (in the actual calculation in [9] static terms seem to be also considered). In this paper, we follow the calculation as proposed in [9]. Therefore, only the heat flux change due to a change in ECH heating power will be considered such that transport can be considered around an equilibrium. Then, a heating power perturbation can be expressed as $P\left(\rho,t\right) \approx P_0\left(\rho\right) + \tilde{P}\left(\rho,t\right)$, which induces a perturbation in the temperature $T_e\left(\rho,t\right) \approx T_0\left(\rho\right) + \tilde{T}_e\left(\rho,t\right)$ and in the heat flux $q_e\left(\rho,t\right) \approx q_0\left(\rho\right) + \tilde{q}_e\left(\rho,t\right)$. The quantities $P_0\left(\rho\right)$, $T_0\left(\rho\right)$, and $q_0\left(\rho\right)$ denote the (static) equilibrium profiles, which are linked such that they satisfy (1) in steady state. $\tilde{P}\left(\rho,t\right)$, $\tilde{T}_e\left(\rho,t\right)$, and $\tilde{q}_e\left(\rho,t\right)$ denote the perturbations around this equilibrium. Considering only the perturbed quantities (1) simplifies to

$$\frac{\partial}{\partial t}\left(n_e \tilde{T}_e\left(\rho,t\right)\right) = \nabla_\rho\left(-\tilde{q}_e\left(\rho,t\right)\right) + \tilde{P}\left(\rho,t\right). \qquad (2)$$

The next step is determining the perturbative heat flux from this equation. Therefore, the expression in [9] is formulated in the cylindrical coordinate system using a notation consistent with this paper, i.e.,

$$\tilde{q}_e\left(\rho,t\right) = -\frac{1}{\rho}\int_0^\rho \rho^\star\left(\frac{\partial}{\partial t}\left(n_e \tilde{T}_e\left(\rho^\star,t\right)\right) - \tilde{P}\left(\rho^\star,t\right)\right) d\rho^\star, \qquad (3)$$

$\tilde{q}_e\left(\rho,t\right)$ describes the change of $q_e\left(\rho,t\right)$ due to a perturbation $\tilde{P}\left(\rho,t\right)$. Note that in practice the difference in using T_e or $\tilde{T}_e$ and $P\left(\rho,t\right)$ or $\tilde{P}\left(\rho,t\right)$ is an offset in the absolute value of the heat flux, both vertical and horizontal. However, using T_e or $P\left(\rho,t\right)$ does not modify the shape of the Lissajous curve itself. Moreover, we have omitted the 3/2 term as it has no impact on the discussions.

The main question is now are the perturbations under experimental conditions small enough such that (2) can be considered linear and consequently also the so-called "hysteresis in flux" observations.

2.2. Perturbative experiments generally result in linear perturbations

The fundamental idea of perturbative experiments is to have a sufficiently small perturbation such that the

resulting response can be considered linear [22]. For the experiments in which the so-called "hysteresis in flux" behavior (Lissajous curve) is observed (mainly stellarators), we conclude that this linearity condition has been largely satisfied based on the following scientific evidence:

(i) In W7-AS the two-tone linearity test, i.e., the existence of intermodulation frequencies induced by non-linearities, showed no sign of a non-linearity [11].

(ii) In LHD under similar conditions as the observations in [9], the two-tone linearity test showed only a weak non-linearity, which was $1 \sim 2$ orders smaller than the main perturbation component [10].

(iii) Step responses at W7-AS show that at some distance to the deposition profile the temperature responses are linear and close to the deposition profile the temperature responses are non-linear [23]. As such at some distance to the source the linearity condition is satisfied.

(iv) The P dependence of χ_e as reported in [24, Fig. 11] is a smooth function of $P \sim P^{0.6}$, i.e., linearizable.

(v) The $q_P(P)$ dependence shown in [9, Fig. 6] is also smoothly decreasing when the power decreases.

(vi) According to [12] "there is overwhelming evidence in the literature that the response of the plasma to a perturbation is linear or nearly so" for transport experiments.

From the observations in LHD and W7-AS, we conclude that although some non-linearities are detected, the so-called "hysteresis in flux" behavior originates from a dominantly linear behavior as the non-linearities found are only present close to the deposition location and are very weak outside this region. Moreover, the smooth dependence on P of transport (v) also implies that there exists a sufficiently small perturbation for which the transport can be modeled fully linear.

Conclusion *Observed "hysteresis in flux" behavior (Lissajous curves) must be reproducible by a linear model*

Consequently, from the literature we conclude that $\tilde{T}_e(\rho,t)$ and $\tilde{q}_e(\rho,t)$ can be considered as a linear response to a ECH perturbation $\tilde{P}(\rho,t)$. This is a crucial step in the analysis as the transport phenomena that can reproduce the Lissajous curves must be reproducible by a linear model (as we will show in the next section). In this paper, we discuss two possible explanations for the observed Lissajous curves: a) errors in the estimation of the deposition profiles results in errors in the heat flux reconstructions; and b) a direct non-local dependence of transport on the heating power by connecting various models found in the literature.

3. Apparent instantaneous transport due to errors in the estimation deposition profile

The previous section infers from the literature that the observational part in perturbative experiments are dominantly linear. Hence, one of the explanations suggested in the literature to explain a direct dependence of transport on heating, is a deposition profile which is much broader than expected from ray-tracing calculations [11, 18]. Hence, we study the following proposition:

Proposition *If a simulated error in the deposition profile estimate can reproduce the experimentally observed Lissajous curves, then such errors must, at least partly, contribute to the experimentally observed Lissajous curves*

The consequences of errors in the estimation of the deposition profile, i.e., errors in ray-tracing calculations, will be investigated in this section.

3.1. Methodology and simulation design

That an error can be responsible for the experimentally observed Lissajous curves can be shown by introducing such an error in a simulation. Therefore, we simulate (2) in cylindrical coordinates

$$n_e \frac{\partial \tilde{T}_e(\rho,t)}{\partial t} = n_e \frac{1}{\rho}\frac{\partial}{\partial \rho}\left(\rho \chi_e \frac{\partial \tilde{T}_e(\rho,t)}{\partial \rho}\right) + P_{ech}(\rho,t)\,\tilde{U}(t), \quad (4)$$

where the real deposition profile $P_{ech}(\rho)$ and the time dependent part $\tilde{U}(t)$ have been separated. In this case, $\tilde{U}(t)$ is a symmetric block-wave with a modulation frequency of 25 Hz. The boundary conditions for this simulation are $\nabla_\rho \tilde{T}_e(0,t) = 0$ and $\tilde{T}_e(1,t) = 0$ ($a = 2.2$ [m] (ITER geometry), $\rho = r/a$, r is the radius in [m]). Both the electron density $n_e = 2.1 \cdot 10^{19}$ [m^{-3}] and the electron heat diffusion coefficient $\chi_e = 8$ [m^2/s] are chosen homogeneous for tractability of the results. Choosing non-homogeneous profiles for χ_e and n_e will not change the outcomes of the analysis. Note that the $\nabla_\rho-$operator is used, simplifying the notation, to denote the spatial derivative $\partial/\partial\rho$. Three different simulations are performed using different deposition

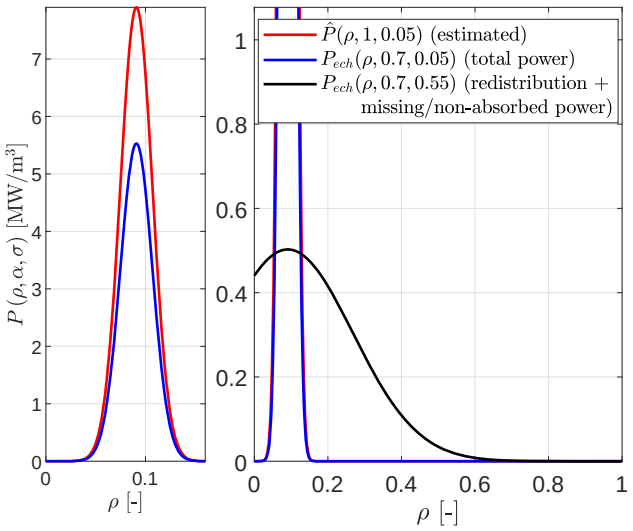

Figure 1. Deposition profiles used to simulate temperature profiles and deposition profile used to estimate the heat flux. The simulated deposition profiles use following values $P_{ech}(\rho) = P_{dep}(\rho, 0.7, 0.05)$ (blue), $P_{dep}(\rho, 0.7, 0.55)$ (black). The deposition profile used to estimate the heat flux is given by $\hat{P}(\rho) = P_{dep}(\rho, 1, 0.05)$ (red).

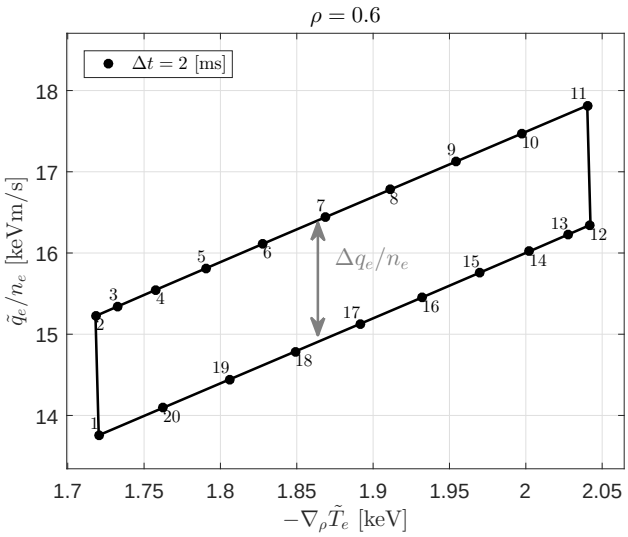

Figure 2. Time evolution of the heat flux $\tilde{q}_e$ versus $\nabla_\rho \tilde{T}_e$ at radial location $\rho = 0.6$ based on broadening . The Lissajous curve further away from the source at $\rho = 0.6$ with $\chi = 8$ [m^2/s]. The deposition used to simulate is $P_{ech}(\rho) = P_{dep}(\rho, 0.7, 0.55)$ and to estimate $\hat{P}(\rho) = P_{dep}(\rho, 1, 0.05)$. Both can also be found in Fig. 1. To calculate the diffusion coefficient multiply the slope by $a = 2.2$. *Notice its resemblance to [9, Fig. 5].*

profiles all using following parameterization

$$P_{dep}(\rho, \alpha, \sigma) = \alpha \cdot P_m \cdot \frac{1}{\sigma\sqrt{\pi}} \exp\left(-\frac{(\rho - \rho_{dep})^2 a^2}{\sigma^2}\right). \tag{5}$$

The deposition profile $P_{dep}(\rho)$ is defined by a Gaussian function where $P_m = 0.7$ [MW/m^2], $\rho_{dep} = 0.1$ the center of deposition, and the dispersion σ [m]. Then, (4) is simulated using an explicit finite difference code [25]. As ρ does not have a unit, it is multiplied by a.

The deposition profile used to estimate the heat flux is called $\hat{P}(\rho)$ such that $\tilde{P}(\rho, t)$ in (3) is defined as

$$\tilde{P}(\rho, t) = \hat{P}(\rho)\tilde{U}(t). \tag{6}$$

Fig. 1 shows both the deposition profile used to estimate the heat flux is called $\hat{P}(\rho)$ and those that are used to simulate the temperature profiles $P_{ech}(\rho)$.

In practice, first (4) is simulated by setting α and σ in (5). The heat flux is then calculated using (3) and (6) where for P_{dep} a different α and σ are used. In other words, in these simulations, at the deposition location in (4), a difference in α means that part of the energy has never reached the plasma, known as 'missing power' [6], and a difference in σ that energy is deposited at a different spatial location than expected.

3.2. Lissajous curves based on deposition estimation errors

This section shows that the experimentally observed Lissajous curves can be reproduced using an error in the deposition profile as is shown in Fig. 2. To understand this, first we split (3) used to calculate the heat flux into two components, i.e.,

$$\tilde{q}_e(\rho, t) = \tilde{q}_{\partial T/\partial t} + \tilde{q}_P, \tag{7}$$

where the heat flux contribution directly related to the temperature is given by

$$\tilde{q}_{\partial T/\partial t}(\rho, t) = -\frac{1}{\rho}\int_0^\rho \rho^\star n_e \frac{\partial \tilde{T}_e}{\partial t} d\rho^\star \tag{8}$$

and that of the heat source by

$$\tilde{q}_P(\rho, t) = \frac{1}{\rho}\int_0^\rho C \cdot \rho^\star \cdot \hat{P}(\rho^\star)\tilde{U}(t)\, d\rho^\star. \tag{9}$$

The constant $C = 6.24 \cdot 10^{24}$ is the conversion factor from [MWm^{-3}] to [keVs^{-1}m^{-3}]. As $\tilde{U}(t)$ is a block-wave, $\tilde{q}_P$ will also be a block-wave function because the integral in (9) is only applied over the spatial coordinate $\rho^\star$ and not over time. Consequently, in case $\hat{P}(\rho) = P_{ech}(\rho)$ the discontinuities introduced by the block-wave modulation at the ECH turn on/off moment and location, need to be canceled out by a discontinuity in $n_e \partial \tilde{T}_e/\partial t$ such that $\tilde{q}_e$ versus $\nabla_\rho \tilde{T}_e$ results in a line with slope the diffusion coefficient. Hence, the assumed heat flux model (4) is exactly reproduced as is shown in Fig. 3 (validation). However, if there is a difference between $\hat{P}(\rho)$ and $P_{ech}(\rho)$, the discontinuities in $\hat{P}(\rho)$ and $n_e \partial T_e/\partial t$ no longer cancel each other out resulting in a discontinuity in

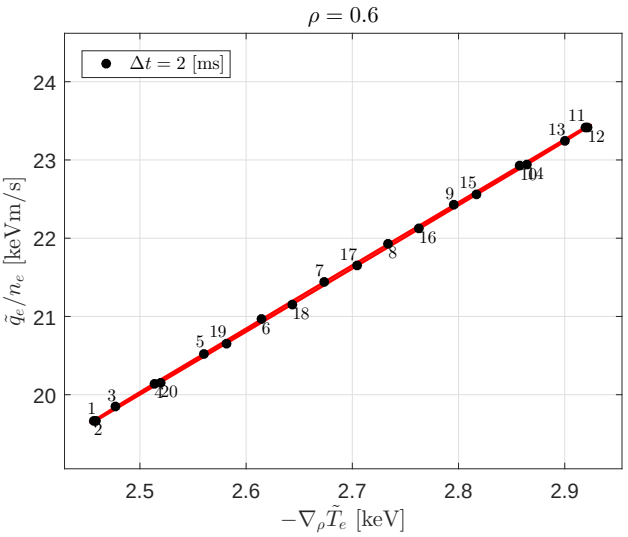

Figure 3. Time evolution of the heat flux $\tilde{q}_e$ versus $\nabla_\rho \tilde{T}_e$ at radial location $\rho = 0.6$ when there is no difference between the estimated and used deposition profile where $\chi = 8$ [m^2/s]. The deposition profile used to simulate and estimate is $P_{ech}(\rho) = \hat{P}(\rho) = P_{dep}(\rho, 1, 0.05)$. Both can also be found in Fig. 1. To calculate the diffusion coefficient multiply the slope by $a = 2.2$.

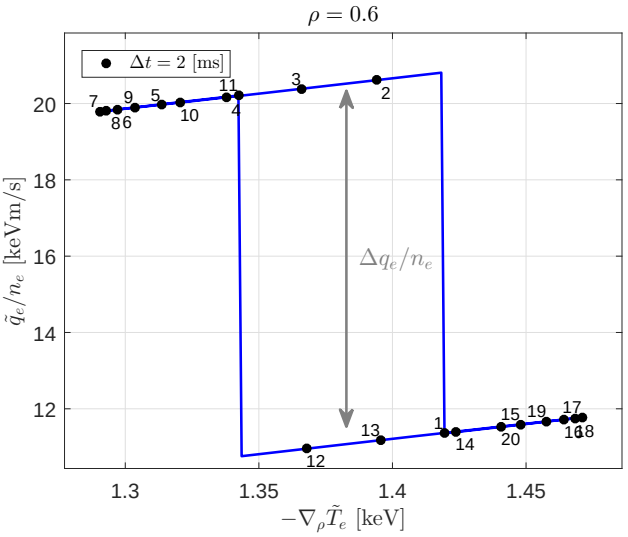

Figure 4. Time evolution of the heat flux $\tilde{q}_e$ versus $\nabla_\rho \tilde{T}_e$ at radial location $\rho = 0.6$ based on a total power error only. The Lissajous curve further away from the source at $\rho = 0.6$ with $\chi = 8$ [m^2/s]. The deposition used to simulate is $P_{ech}(\rho) = P_{dep}(\rho, 0.7, 0.05)$ and to estimate $\hat{P}(\rho) = P_{dep}(\rho, 1, 0.05)$. Both can also be found in Fig. 1. To calculate the diffusion coefficient multiply the slope by $a = 2.2$.

$\tilde{q}_e$. Depending on the difference between $\hat{P}(\rho)$ and $P_{ech}(\rho)$, the discontinuity will occur at different time instances. Thereby showing that a deposition error over a very broad profile is necessary. This is shown in Fig. 4 and Fig. 2. Note that all the corresponding Lissajous curves are color coded according to the color coding used in Fig. 1.

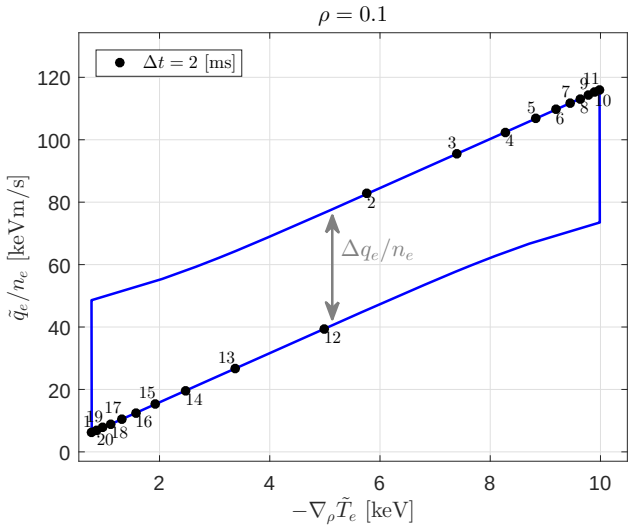

Figure 5. Time evolution of the heat flux $\tilde{q}_e$ versus $\nabla_\rho \tilde{T}_e$ at radial location $\rho = 0.1$ based on a total error only where $\chi = 8$ [m^2/s]. The deposition used to simulate is $P_{ech}(\rho) = P_{dep}(\rho, 0.7, 0.05)$and to estimate $\hat{P}(\rho) = P_{dep}(\rho, 1, 0.05)$. Both can also be found in Fig. 1. To calculate the diffusion coefficient multiply the slope by $a = 2.2$.

Fig. 4 shows already some similarity to experimentally observed Lissajous curves [9, Fig. 5]. However, the discontinuities occur at different time instances as observed experimentally. It has excursions, the points 04-11 and 14-01 outside the closed loop. In other words, the moment $\tilde{q}_{\partial T/\partial t}(\rho, t)$ switches is delayed with respect to when $\tilde{q}_P(\rho, t)$ switches. This delay can be quantified by the time that has passed between number 4 and number 11 (and number 14 to 01), which corresponds to 14 [ms]. Equivalently, the delay is the moment the curve changes direction in this case between 01 and 07 and 11 and 18. This is approximately one third of the period (25 Hz) with a distance of $\Delta\rho \approx 0.55$ [-] to the source in cylindrical geometry. However, this is precisely what is *not* being observed in the experiments at these spatial locations. Hence, to be able to reproduce what is experimentally is observed, this delay needs to be removed. An analytic calculation of the delay in slab-geometry can be found in Appendix B.

Therefore, consider the estimate of $\tilde{q}_e(\rho, t)$ at a smaller radius first $\rho = 0.1$, which is shown in Fig. 5. Then, we see almost an exact representation of the experimentally observed Lissajous curves. However, as we also observe this at larger radii, it means that a heating term must be present all radii. This has been simulated in Fig. 2 perfectly reproducing the experimental Lissajous curves in [9, Fig. 5].

Conclusion *Errors in the estimation of deposition profile can reproduce the observed Lissajous curves* ***only*** *when there is a very broad deposition profile*

This means that when redistributing heating power over the entire domain reproduces the Lissajous curves modeled in [24] and observed in experiments [9] exactly. This can also be further analyzed by plotting $\tilde{q}_{\partial T/\partial t}(\rho,t)$ and $\tilde{q}_P(\rho,t)$, separately, as is done in Fig. 6. As (7) shows the sum of $\tilde{q}_{\partial T/\partial t}(\rho,t)$ and $\tilde{q}_P(\rho,t)$ should be exactly zero in case there is no redistribution or missing power. However, if there is a height difference between $\tilde{q}_{\partial T/\partial t}/n_e$ ($\Delta\tilde{q}_{\partial T/\partial t}/n_e$) and $\tilde{q}_P/n_e$ ($\Delta\tilde{q}_P/n_e$), the resulting Lissajous curve of $\tilde{q}_e/n_e$ opens up in Fig. 2, i.e., $\Delta\tilde{q}_e/n_e \neq 0$. In which direction the Lissajous curve opens up (direction of rotation) depends on the radial location and on the amount of missing power and/or non-absorbed power. The heat flux contribution due to $\tilde{q}_P/n_e$ will simply be a block-wave function, which appears as a square with a clockwise rotation in Fig. 6(a). Hence, the opening can be fully attributed to a difference between what is assumed as heating deposition profile and what the slow (diffusive) transport considers to be the deposition profile later called the effective heating deposition profile P_{eff}.

The Lissajous curve based on the heat source in Fig. 6(a) has a remarkable resemblance to [9, Fig. 7], the so-called "hysteresis in turbulence" [9]. However, Fig. 6(a) has again nothing to do with hysteresis. It is merely a block-wave plotted against a function which changes direction at the same moment ($\mathrm{sign}\left(\partial\left(\partial T_e(\rho,t)/\partial\rho\right)/\partial t\right) = \mathrm{sign}\left(\partial P(\rho,t)/\partial t\right)$). Hence, the so-called hysteresis in turbulence [9] is merely a block-wave as can be seen in [9, Fig. 3, An] plotted against $\partial T_e/\partial\rho$. However, what is remarkable is that the turbulence level is switching with heating power and not changing as function of $\partial T_e(\rho t)/\partial\rho$, which suggests that the Lissajous curves observed in $\tilde{q}_e(\rho,t)$ are not merely the result of an error in the ray-tracing.

3.3. Time-scale separation

In this section, we show that it is possible to split transport in a slow and fast time-scale. This can be best understood by increasing the diffusion coefficient (slow time-scale), thereby showing that the fast time-scale cannot be reproduced by changing the diffusion coefficient. This is shown in Fig. 7 where the diffusion coefficient has been increased to $\chi = 100$ [m^2/s].

Although the shape of the Lissajous curves are very similar to those observed in [9, Fig. 5] and Fig. 2 the slopes are very different. In [9, Fig. 5] the slope is approximately $\chi = 8$ [m^2/s] and not $\chi = 100$ [m^2/s] . In other words, the slow transport component related to the slopes in the Lissajous curves will be modified. Moreover, increasing the transport coefficients yields also a number of problems in the time evolution of T_e, $\nabla_\rho T_e$, and $\partial T_e/\partial t$, as they will become much larger than observed in experiments (not shown here). Hence, this brings us to an important conclusion that the slow time-scale of transport (in a linear sense) cannot be used to reproduce the observed Lissajous curves. Therefore, a fast time-scale is necessary, which is here an instant (static) error on the deposition profile used to calculate the heat flux. Hence, transport can be split in two components as is presented in Fig. 8. The crucial question is if such broad deposition profiles are feasible. In other words, are ray-tracing predictions so far off. Although we cannot exclude such broad deposition profiles, there is an alternative explanation through the use of non-local models, which we will show to have exactly the same mathematical structure in a linear sense as presented in Fig. 8.

4. Non-local dependence of transport

This section discusses two different local dependencies of the heat flux q_e proposed for stellarators, including some extensions. As will be shown these also reproduce the Lissajous curves in [9, Fig. 5] and Fig. 2. The non-local models discussed in this section are based on indirect measurement observations and direct calculations of the heat flux q_e.

4.1. Non-local based transport models in stellarators (literature)

The common heat flux model proposed to incorporate power dependency and power degradation in W7-AS is based on an electron diffusivity χ_e being dependent on the power. This results in the following model for the electron heat flux [24]

$$q_e = -n_e\chi_e(P)\nabla_\rho T_e. \tag{10}$$

This model is based on a number of important observations in W7-AS:

(i) The step response for an up- and downward step in P is different implying different values for χ_e for different power levels [4].

(ii) Dependencies of χ_e on T_e are excluded and a dependency of χ_e on $(\nabla_\rho T_e)^\alpha$ for $\alpha > 0.5$ is also excluded [24].

(iii) χ_e dependence on P is in accordance with the scaling law dependencies of the confinement time τ_e on P ($\chi \sim P^{0.6}$) [4].

(iv) χ_e calculated in steady-state $\left(\chi_e^{PB}\right)$ is similar to the one calculated using a perturbation $\left(\chi_e^{HP}\right)$ for a specific power level [5].

(v) Both χ_e^{PB} and χ_e^{HP} depend on the input power for both off-axis and on-axis deposition profiles [1, 24].

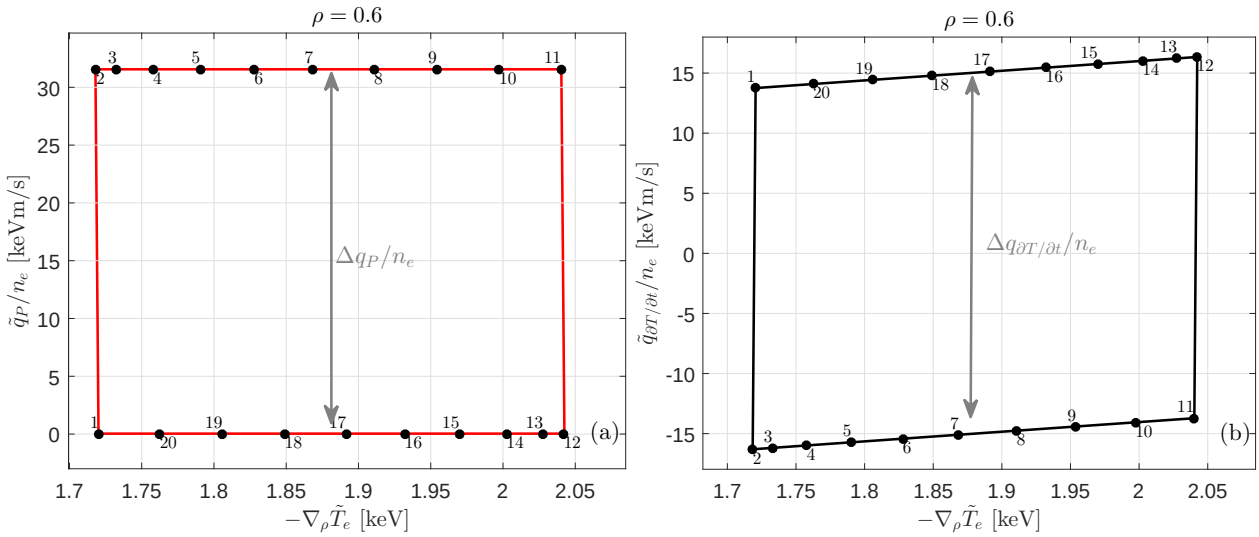

Figure 6. Lissajous curves of the heat flux (a) $\tilde{q}_P(\rho,t)$ (b) $\tilde{q}_{\partial T/\partial t}(\rho,t)$ versus $-\nabla_\rho T_e$ in the case where the deposition used to simulate is $P_{ech}(\rho) = P_{dep}(\rho, 0.7, 0.55)$ and to estimate $\hat{P}(\rho) = P_{dep}(\rho, 1, 0.05)$. $\hat{P}(\rho)$ will always be the same and hence the heat flux will be $\tilde{q}_P(\rho,t)$ (red).

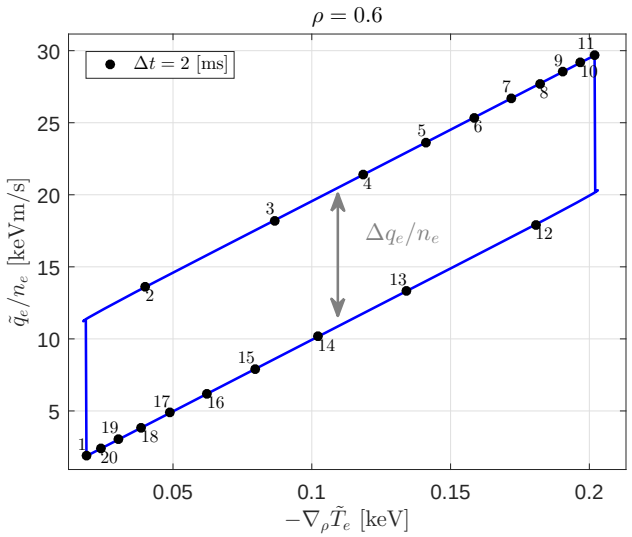

Figure 7. Time evolution of the heat flux $\tilde{q}_e$ versus $\nabla_\rho \tilde{T}_e$ at radial location $\rho = 0.6$ based on a total power error only. The Lissajous curve further away from the source at $\rho = 0.6$ with $\chi = 100$ [m^2/s]. The deposition used to simulate is $P_{ech}(\rho) = P_{dep}(\rho, 0.7, 0.05)$ and to estimate $P_{est}(\rho) = P_{dep}(\rho, 1, 0.05)$. Both can also be found in Fig. 1. To calculate the diffusion coefficient multiply the slope by $a = 2.2$.

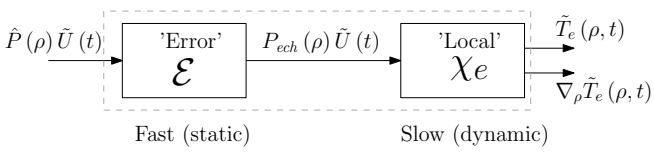

Figure 8. Block diagram showing how the fast (static) time-scale is affected for an error in the deposition profile.

In LHD the heat flux q_e has been estimated by expressing the heat equation (1) in terms of q_e [9]. The resulting $q_e - \nabla_\rho T_e$ Lissajous curve in [9, Fig. 5] suggests that the diffusion coefficients are the same when the power is on or off, i.e., the slopes are the same when the power is constant. The modeling in [26][27, eq. 6]

$$q_e = q_{jump} - n_e \chi_e \nabla_\rho T_e, \tag{11}$$

is based on this observation, where q_{jump} is an artificially introduced quantity to explain the jumping of the heat flux when the heating power is turned on or off and is interpreted as non-linear hysteresis behavior [9, 27]. As a consequence, this model does not take the heating power dependence of q_{jump} explicitly into account (see also section 2.2 in [28]).

The observational model in (11) is different from (10) in that it shows 1) that the 'slow' slopes in the $q_e - \nabla_\rho T_e$ plane are equal instead of changing with power levels; and 2) that there is an extra variable q_{jump}, which needs to be taken into account.

Concerning the type of discharges discussed here, it is important to mention that for both W7-AS and LHD they are low-density discharges [4, 9]. However, there are also strong indications that such observations are not limited to low-density plasmas only. Also important to mention is that the here discussed observations were made in both plasmas with only EC heating (W7-AS) and plasmas dominated by NBI heating (LHD) [4, 9].

Finally, the reason why other non-local models have not been discussed here is that they often try to model a non-local diffusivity, e.g., through a fractional diffusion model [14, 15]. However, as the observations

in LHD clearly show the diffusion coefficients (slopes) are hardly affected, it is unclear how these would fit in the context discussed here.

4.2. Extended heat flux model

Here, the two models in (10) and (11) will be unified and its implications are discussed. The first step is to go from an observational q_{jump} to a descriptive dependency of the heat flux. First of all, q_{jump} in [9, Fig. 6] depends on the change of the input power P. Hence, we replace q_{jump} by $q_P(P)$ in (11). This extension gives the heat flux model more generality as this model can also be used to describe other power modulation wave-forms such as sinusoidal and ternary modulations, whereas q_{jump} is limited to block-wave modulations.

It is unclear whether χ_e should be made dependent of P in the joint model of q_e. On one hand, the χ_e dependence on P is supported by the observations at W7-AS and static predictions at both LHD [29] and TJ-II [30, 31]. On the other hand, the LHD observation in [9, Fig. 5] does not show such a dependence. However, new experimental results show that such a dependence may exist [32]. Hence, the dependence of χ_e on P remains an open question to be resolved but for completeness we have included this dependence in the overall non-linear heat flux model

$$q_e(\rho,t) = q_P(\rho, P(\cdot,t)) - n_e\chi_e(\rho, P(\cdot,t))\nabla_\rho T_e, \quad (12)$$

where $q_e(\rho,t)$ is a function of the whole power density profile $P(\cdot,t)$ not the local ρ. Hence, the $(\cdot,t)$ symbol. An example is the following arbitrary dependency of $q_P(\rho, P(\cdot,t))$ on ρ

$$q_P(\rho, P(\cdot,t)) = \int_0^\rho g(\xi)P(\xi,t)d\xi, \quad (13)$$

where, even when $P(\xi,t)$ at ξ is zero, $q_P(\rho, P(\cdot,t))$ is non-zero. In other words, $q_P(\rho,t)$ at a specific radial coordinate ρ does not (only) depend on the value of $P(\rho,t)$, but on the entire deposition profile $P(\cdot,t)$. The same holds for $\chi_e(\rho, P(\cdot,t))$. The spatial dependence of $\chi_e(\rho, P(\cdot,t))$ on $P(\rho,t)$ and $q_P(\rho, P(\cdot,t))$ on $P(\rho,t)$ can be different. Also, it is important to mention that the discussion in [33] concerning so-called missing power also suggests that (10) should be extended with q_P, where missing power is defined as the difference between the total power put into the plasma and total power measured inside the plasma. In [33] it is described that an energy balance analysis at W7-AS showed that only 30% of the so-called missing power can be recuperated by a power dependence of χ_e. q_P is a mechanism to explain this so-called missing power.

Fig. 9 shows the dependencies of q_e on P and $n_e\nabla_\rho T_e$ for (12) using a power dependence of $\chi_e \sim P^{0.6}$ and $q_P \sim P^{0.5}$ similar to scaling law dependencies [24]. The symmetric block-wave modulation is shown in Fig. 9(b) where the blue and red dots show the points where power steps occur and the black dots show the slow evolution. Fig. 9(a) shows the non-linear dependence of q_e on P and $n_e\nabla_\rho T_e$ and how q_e changes under influence of a symmetric block-wave power modulation. The surface of q_e is smooth and the evolution over the surface differs depending on how the input P is chosen. A step occurs in the power in case a symmetric block-wave modulation is used at the locations that the power is turned on or off. This must also occur on the 2D-plane in Fig. 9(a). After the heating has been turned on, P stays the same and as such the profiles evolve on a slow time-scale according to χ_+^{HP} until the point the heating is turned off again. Then, a slow evolution according to χ_-^{HP} occurs. Note that, in case of the LHD observations it is suggested that χ_-^{HP} and χ_+^{HP} are the same [9].

In Fig. 9(c) the projection of this 2D-dependence in the $q_e - \nabla_\rho T_e$ plane is shown. This results in the Lissajous curve as has been presented in [24, Fig. 17], observed in [9, Fig. 5], and which have been simulated in Fig. 2. Depending on the sensitivity of q_P on P and χ_e on P, the size of the vertical step will be changing in Fig. 9(c). Moreover, the $\chi_e(P)$ dependency will determine how much the slopes will be changing. Fig. 9(d) shows the projection in the $q_e - P$ plane, which shows a similar Lissajous curve. The projection in Fig. 9 also implies that if P is not stepping, but for instance is a sinusoid, then the Lissajous curves will look entirely different. In the case of a sinusoid, the Lissajous curves will become ellipsoids (not shown here). This also holds for Fig. 2 as there are no steps in a sinusoid. Hence, showing the equivalence between assuming a fast component in the heat flux and a broadening of the deposition profile.

4.3. Perturbative experiment and linearized heat transport model

As the dependence of $q_P(\rho, P(\rho,t))$ and $\chi_e(\rho, P(\rho,t))$ on $P(\rho,t)$ are unknown, a generalized derivative is used known as the Fréchet derivative [34, Def A.s.25]. Hence, the linearized heat flux model for $\tilde{q}_e(\rho,t)$ of (12) is given by

$$\begin{aligned}\tilde{q}_e(\rho,t) = &\left(\left(\frac{\partial q_P}{\partial P}(\cdot,P_0)\right)\left(\tilde{P}\right)\right)(\rho,t)\\ &-\left(\left(\frac{\partial \chi_e}{\partial P}(\cdot,P_0)\right)\left(\tilde{P}\right)\right)(\rho,t)\; n_e\nabla_\rho T_0\\ &-\chi_e(\rho,P_0(\rho))\, n_e\nabla_\rho\tilde{T}_e. \quad (14)\end{aligned}$$

The full derivation is given in Appendix A including an example of why we need the FrÃ©chet derivatives. In [35] also other linear quantities such as convection

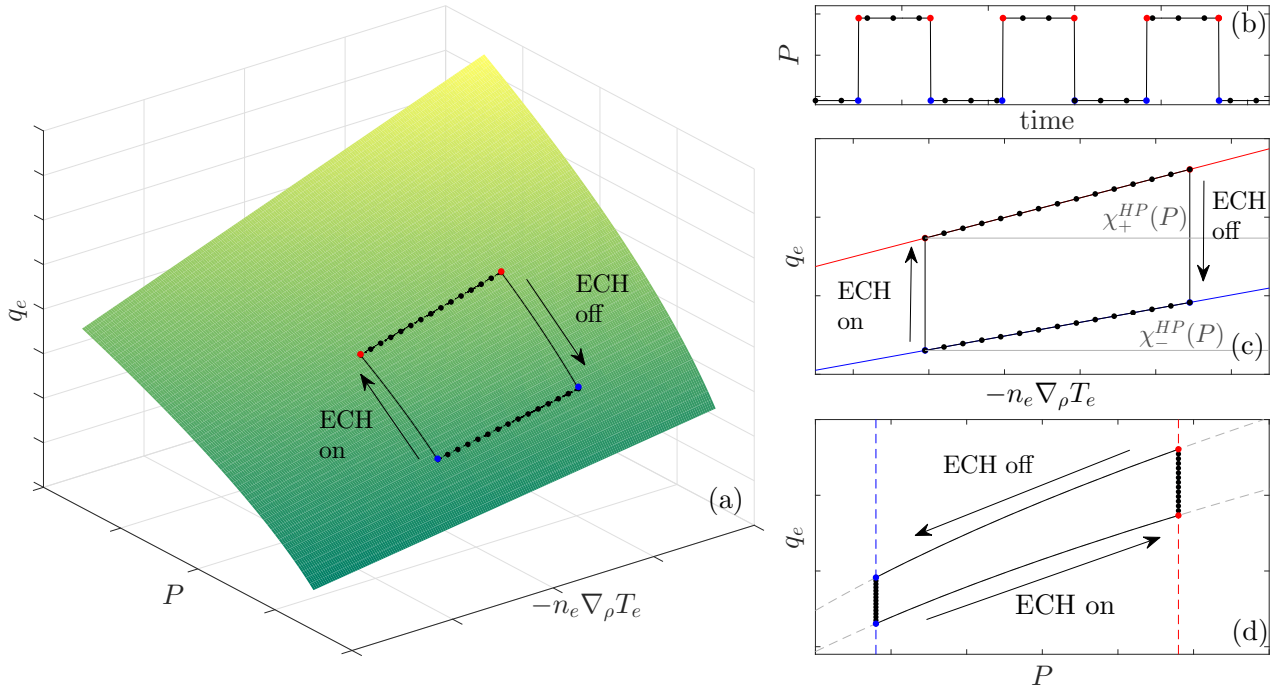

Figure 9. Graphical representation of (12) with (a) Static dependency of the heat flux q_e in terms of P and $n_e\nabla_\rho T_e$ based on (12) with in black the time dependent heat flux evolution due to a symmetric block-wave where the red and blue dots the locations a step occurs. (b) Symmetric block-wave perturbation where the blue and red the points are the time instances the block-wave steps. (c) The Lissajous curve of the time evolution of the block-wave, with in red χ_+^{HP} and blue χ_-^{HP} the two different slopes due to the power dependent diffusivity. (d) The power dependence of the heat flux due to a symmetric block-wave input. The heat flux changes on a fast time scale with heating power.

and damping appear in the heat equation, which could also be further extended with other non-linear dependencies. However, as the observations in [4, 9] give no indication that such terms are necessary they are not considered here. As (2) describes a linearized equation, the time and deposition part can be separated in (14) using

$$\tilde{P}\left(\rho,t\right)=P_{ech}\left(\rho\right)\tilde{U}\left(t\right) \tag{15}$$

such that

$$\left(\left(\frac{\partial q_P}{\partial P}\left(\cdot,P_0\right)\right)\left(\tilde{P}\right)\right)\left(\rho,t\right)= \left(\left(\frac{\partial q_P}{\partial P}\left(\cdot,P_0\right)\right)\left(P_{ech}\right)\right)\left(\rho\right)\tilde{U}\left(t\right) \tag{16}$$

and

$$\left(\left(\frac{\partial \chi_e}{\partial P}\left(\cdot,P_0\right)\right)\left(\tilde{P}\right)\right)\left(\rho,t\right)= \left(\left(\frac{\partial \chi_e}{\partial P}\left(\cdot,P_0\right)\right)\left(P_{ech}\right)\right)\left(\rho\right)\tilde{U}\left(t\right). \tag{17}$$

This allows the heat flux $\tilde{q}_e$ to be rewritten as

$$\tilde{q}_e(\rho,t)=q_{\mathcal{T}}\left(\rho,P_{ech}\right)\tilde{U}\left(t\right)-\chi_e\left(\rho,P_0(\rho)\right)n_e\nabla_\rho\tilde{T}_e, \tag{18}$$

where

$$q_{\mathcal{T}}\left(\rho,P_{ech}\left(\rho\right)\right)=\left(\left(\frac{\partial q_P}{\partial P}\left(\cdot,P_0\right)\right)\left(P_{ech}\right)\right)\left(\rho\right) -\left(\left(\frac{\partial \chi_e}{\partial P}\left(\cdot,P_0\right)\right)\left(P_{ech}\right)\right)\left(\rho\right)n_e\nabla_\rho T_0. \tag{19}$$

In the literature various similar (additional) heat flux contributions appear such as q_{offset} [12], also called the heat pinch term q_{pinch} [33], and q_1 [6, p. 3]. These $q-$terms should not be confused with the term $q_{\mathcal{T}}$ because q_{offset}, q_{pinch}, and q_1 (see references) do not depend on the power modulation, whereas $q_{\mathcal{T}}$ does. Note that the fast transport component cannot be explained by critical gradient models, based on the assumption that turbulent modes are driven unstable when $\nabla_\rho T_e$ exceeds a critical value [17, 36, 37, 38, 39]. The reason is that it only acts on the slow time scale. However, critical gradients models can impact the slow transport scale. In such cases the analysis presented here is valid except for a linearization at the specific transition point (between slopes). Moreover, in case χ is considered to be continuously dependent on $\nabla_\rho T_e$ the resulting linearization will be the same as in (18). The reason is that the linearization of $\chi_e\left(\nabla_\rho T_e\right)$ results in the following two additional contributions: 1) an extra contribution to the equilibrium, which

we do not consider; and 2) a contribution equal to $\chi_e \nabla_\rho \tilde{T}_e$, which has already been included in (18) (see also [12]). Moreover, as only the electron channel is directly perturbed and the electron temperature is studied, interactions with other transport channels such as the ion temperature are not considered. Note that only feedback interactions with other channels can give an additional contribution, i.e., interactions where $\tilde{P}(\rho,t)$ or the electron transport itself modifies other transport channels which subsequently modify the electron transport. As this is an even more complicated interaction we will not explicitly analyze it here.

4.4. Re-expressing fast (non-local) transport in effective deposition profile

This section shows that $q_{\mathcal{T}}$ can be mathematically re-expressed as a new deposition profile. Therefore, the linearized perturbative heat flux (18) is substituted back into the heat equation in (2). Then, the time dependent component $\tilde{U}(t)$ can be separated from $q_{\mathcal{T}}$ resulting in the following heat equation

$$\frac{\partial}{\partial t}\left(n_e \tilde{T}_e(\rho,t)\right) = \nabla_\rho\left(\chi_e(\rho, P_0(\rho))\, n_e \nabla_\rho \tilde{T}_e\right) + P_{\mathit{eff}}(\rho)\,\tilde{U}(t), \quad (20)$$

where

$$P_{\mathit{eff}}(\rho) = P_{ech}(\rho) - \nabla_\rho\left(q_{\mathcal{T}}(\rho, P_{ech}(\cdot))\right), \quad (21)$$

where we define $P_{\mathit{eff}}(\rho)$ as the effective heating profile, which is a combination of the actual deposition profile $P_{ech}(\rho)$ and the implicit dependence of the heat flux on this deposition profile $\nabla_\rho(q_{\mathcal{T}}(\rho, P_{ech}(\rho)))$. This also shows that if $q_{\mathcal{T}}$ is non-zero, $q_{\mathcal{T}}$ is perturbed by the source $\tilde{U}(t)$, which in experiments is much faster, than the diffusive (and convective) time-scale. As such it describes fast transport phenomena and other phenomena directly related to the heating source. The apparent deposition profile $P_{\mathit{eff}}(\rho)$ is significantly broader than the real deposition profile as the non-local heat flux occurring at all radii not only those directly perturbed by P_{ech}.

Conclusion *Experimental Lissajous curves can (also) be reproduced by non-local models proposed in the literature*

One may debate if it is better to describe $P_{\mathit{eff}}(\rho)$ directly in terms of a heat flux component $q_{\mathcal{T}}$ as from a physics point of view it is a contribution to the heat flux and not a physical contribution in terms of heating power. However, writing it as (21) gives a dimensionless model description in which the time-scales effectively are separated and comparable

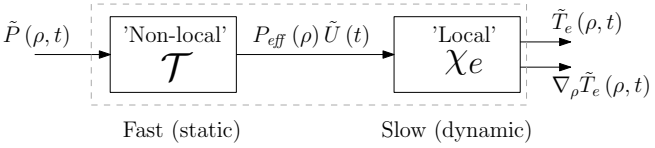

Figure 10. Block diagram of fast transport component caused by non-local transport of linearized transport for time-scales on which the fast transport can be considered static.

to estimates of deposition profiles coming from ray-tracing. This separation can also be seen in Fig. 10, where the $\mathcal{T}$ symbol is used to depict non-local transport. The result shows that non-local transport has exactly the same structure as an error in the deposition profile when linearized. Both a broadening of the deposition profile or non-local transport can have a significant impact on the analysis of transport, which is explained next.

5. Consequences of fast-time scale effects on temperature and transport coefficients

In this section, we discuss how a significant fast-time scale component, be it from an error in deposition profile or non-local transport or both, can be recognized in the measurements. Therefore, we analyze what the effect of the fast component is on the temperature evolution and the harmonic components. Moreover, we show that if a fast time scale component is present, the resulting estimates of transport components (on the slow time-scale) will be erroneous if the time-scales are not properly being separated, which is rarely done in practice.

5.1. Time domain: effect on perturbative temperature profiles

A fast component in the measurements can be recognized in temperature measurements by an absence of delay as explained previously. This means that where the temperature changes direction does not change in time. This can be seen by comparing Fig. 11 without a fast-component and Fig. 12 with such a fast-component. Moreover, the time evolution of the temperature profiles have become more straight, i.e., the derivative $\nabla_t T_e$ is not peaking as much, compared to the temperature evolution without a fast component. Similar changes can be observed in the time evolution of $\partial T_e/\partial t$ and $\partial T_e/\partial \rho$. This straightness and absence of delay can also be appreciated in the time evolution of experimental data as presented in [9, Fig. 3]. Moreover, this is also observed in the responses shown in [4, Fig. 6](W7-AS), where they are more straight than their associated diffusion coefficients based on model simulations.

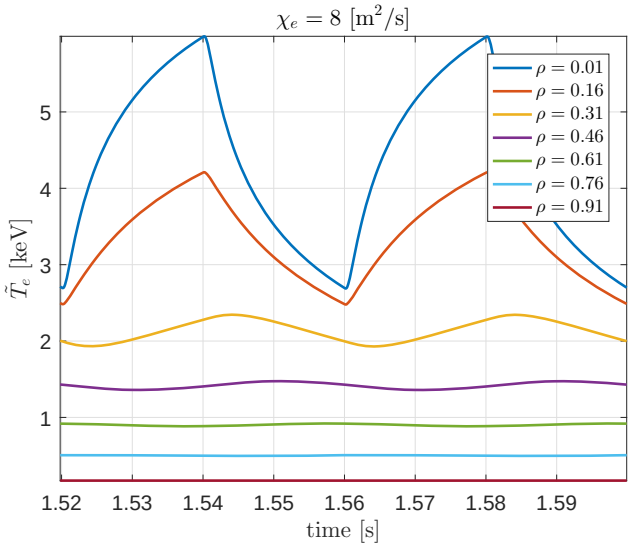

Figure 11. Time evolution of the temperature at different radial locations when using $P_{dep}\left(\rho, 1, 0.05\right)$. They have been simulated with a finite difference simulation using a symmetric block-wave modulation of 25 Hz, the diffusion coefficient is $\chi = 8$ [m^2/s].

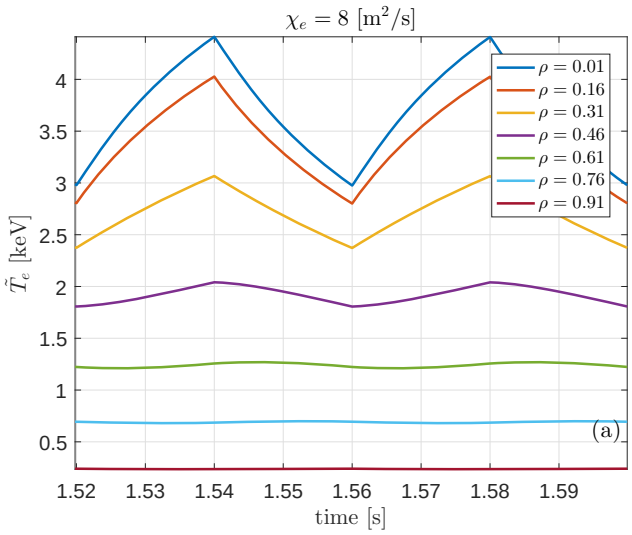

Figure 12. Time evolution's at different radial locations of the temperature when using $P_{dep}\left(\rho, 0.7, 0.55\right)$.

Non-local transport or a broadened deposition profile can also be directly recognized in measurements. The reason is that the perturbation propagates much faster in time when having a non-local transport broadened deposition profile than expected when having diffusive transport only. Consequently, the delay between heat waves (or steps) at different radial locations is small. This is exactly what measurements show in W7-AS [24, 4, Fig. 6]. Here, the delay between a step response in T_e at a radius 5 cm and at the radius of 10 cm is smaller than 0.5 [ms] whereas for $\chi = 1$ [m^2/s] a much larger delay is expected if one only considers diffusion. This delay is equivalent to the phase of the perturbation as is discussed next.

5.2. Frequency domain: effect on the estimated transport coefficients

In frequency domain the presence of an $\mathcal{E}$ and/or $\mathcal{T}$ component is even more apparent as it will result in a reduced spatial decay of the amplitude and phase profiles. This constitutes a problem for the estimation of transport coefficients given the fact that they basically all assume a domain on which no additional heating is present [40, 41, 42]. This effective additional heating is analyzed here, in terms of the amplitude and phase profiles and its effect on the estimation of the transport coefficients.

First, consider the extreme cases of transport without power deposition (in the domain of estimation) and a domain with power deposition but without slow-scale transport ($\chi_e = 0$). If there is no heating power on the semi-infinite domain $[\rho_1, \infty)$ under consideration, then the spatial decay in slab is given by [41](see also Appendix B)

$$\Theta\left(\rho, \omega\right) = \exp\left(-\sqrt{\frac{i\omega}{\chi_e}}\left(\rho - \rho_1\right)\right)\Theta\left(\rho_1, \omega\right), \qquad (22)$$

where $\Theta\left(\rho, \omega\right) = \mathcal{F}\left(T_e\left(\rho, t\right)\right)$ with $\mathcal{F}$ denoting the Fourier transform. On the basis of this simplification transport coefficients can be calculated using [40, 41]

$$\chi_A = \frac{1}{2}\frac{\omega}{\left(A'/A\right)^2} \qquad \text{and} \qquad \chi_\phi = \frac{1}{2}\frac{\omega}{\left(\phi'\right)^2}, \qquad (23)$$

where A'/A is the logarithmic spatial derivative of the amplitude and ϕ' the spatial derivative of the phase. The amplitude and phase as function of ρ in a semi-infinite domain with constant χ_e without a source term are straight lines on a logarithmic scale, where the spatial slope (decay as function of ρ) will become larger with increasing frequency. This follows from (22). Hence, at spatial locations where there is no deposition and at sufficient distance to the boundary for which (22) is a valid solution, which can be seen in Fig. 13 by the solid lines.

The second extreme case is if there is only heating over the entire domain and no (diffusive) transport, then the analytical solution in slab geometry is given by

$$\Theta\left(\omega, \rho\right) = \frac{P_{ech}\left(\rho\right)\tilde{U}\left(\omega\right)}{i\omega}, \qquad (24)$$

where $\tilde{U}\left(\omega\right) = \mathcal{F}\left(\tilde{U}\left(t\right)\right)$. Consequently, if $P_{ech}\left(\rho\right)$ is constant the slope equals zero. If $P_{ech}\left(\rho\right)$ changes with ρ, $\Theta\left(\rho, \omega\right)$ changes exactly the same. If one calculates the diffusion coefficient based on the

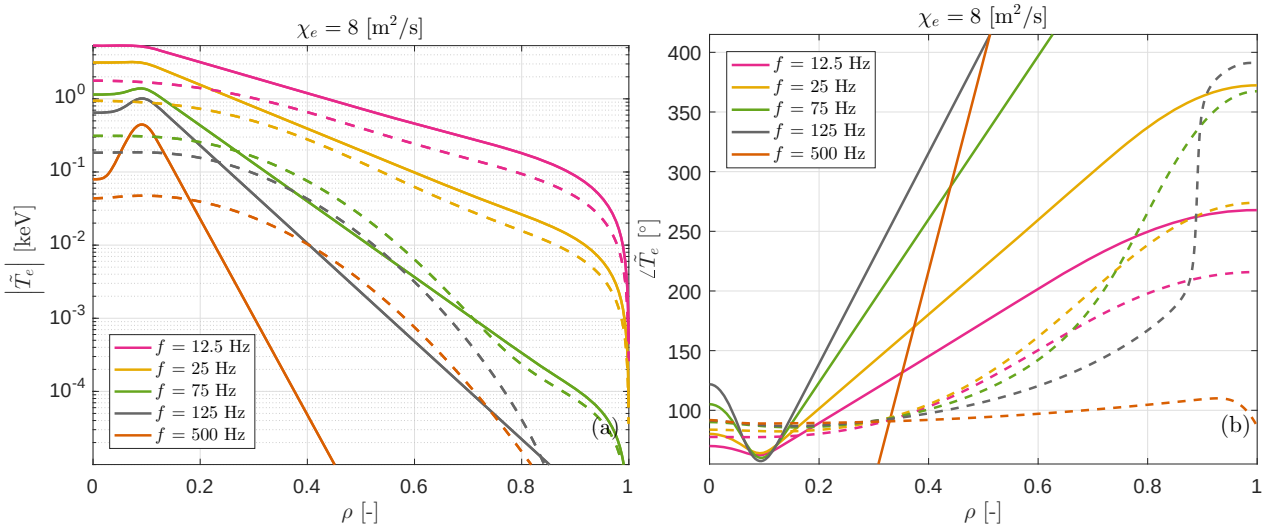

Figure 13. (a) The spatial dependency of the amplitude of the temperature $\left|\tilde{T}_e\right|$ at different frequencies for a narrow deposition profile $\sigma = 0.05$ (lines) and a wide profile $\sigma = 0.55$ (dashed-lines), which corresponds to $\mathcal{T}_r$. (b) The spatial dependency of the phase of the temperature $\angle\tilde{T}_e$ at different frequencies for a narrow deposition profile (lines) and wide deposition profile. If one wants to find the profiles for a specific modulation wave form (symmetric block-wave) simply multiply all the components with the fast Fourier transform of the modulation.

harmonic components of (24) using the assumption that no deposition is present on the domain, i.e., using (23), then with increasing frequency the diffusion coefficient becomes larger. This is because with increasing frequency the slope should become larger in the pure diffusive case, but because there is no change in slope, the diffusion coefficient will need to compensate for this effect.

In reality, the resulting amplitude and phase profiles, and consequently the estimated diffusion coefficients, are the intermediate solution between these extreme cases. This has been simulated using $\hat{P}(\rho) = P_{dep}(\rho, 1, 0.55)$ (5) and a slab geometry instead of cylindrical geometry is used. This avoids an extra ρ dependency. However, the same behavior can be shown for cylindrical geometry. The resulting amplitude and phase profiles are presented in Fig. 13.

The solid lines show the resulting profiles of amplitude and phase for the localized heating. Indeed one can see that they are relatively straight except for the regions close to the boundaries and at the deposition location. However, if the slopes are compared to the profiles belonging to the redistributed or wide profile (dashed lines) one sees directly that they are no longer straight and are lifted up for the amplitude and increase much slower for the phase. Exactly this effect has been observed in several machines [17, 43, 44], where the latter two references also suggest it could be due to hysteresis. This confirms that this effect is not limited to stellarators. In [17], it is also stated that it is probably caused by turbulence. Moreover, the phase behavior becomes also rather difficult to interpret as has been explained in Sec. 5.1.

It is also possible to express the error directly in the diffusion coefficient. Therefore, the relationships in (23) are used, which can be accurately applied as there is no measurement noise and the discretization is very dense. The estimated profiles of χ_e in terms of χ_A and χ_ϕ are shown in Fig. 14. One can now see that the estimated diffusion coefficient will increase with frequency for the wide heating profile, which has also been vaguely noted in [24, Fig. 16]. Moreover, as the semi-infinite domain model has different boundary conditions than used in the simulation, at the boundaries the χ_e estimates are subject to large errors. However, for the narrow deposition profile the diffusion coefficient can be correctly calculated in the central domain. One can also see that the effect on the phase is larger compared to that of the amplitude profiles.

Conclusion *Not taking a wide effective deposition profile into account introduces a significant bias (error) on the estimated transport coefficients*

In summary, these simulations show similar behavior to those measured, but how the actual profiles will look in measurements depends on the exact form of P_{eff}. In the case of high frequency modulation P_{eff} must become visible as diffusion is suppressed. This is also what is observed in the literature, where a broadening of the deposition profile with a factor larger than two is observed compared to the deposition profile according to ray-tracing calculations [18, 19]. In [19] this is studied to find an explanation for the broadening through transport. However, one has to be careful

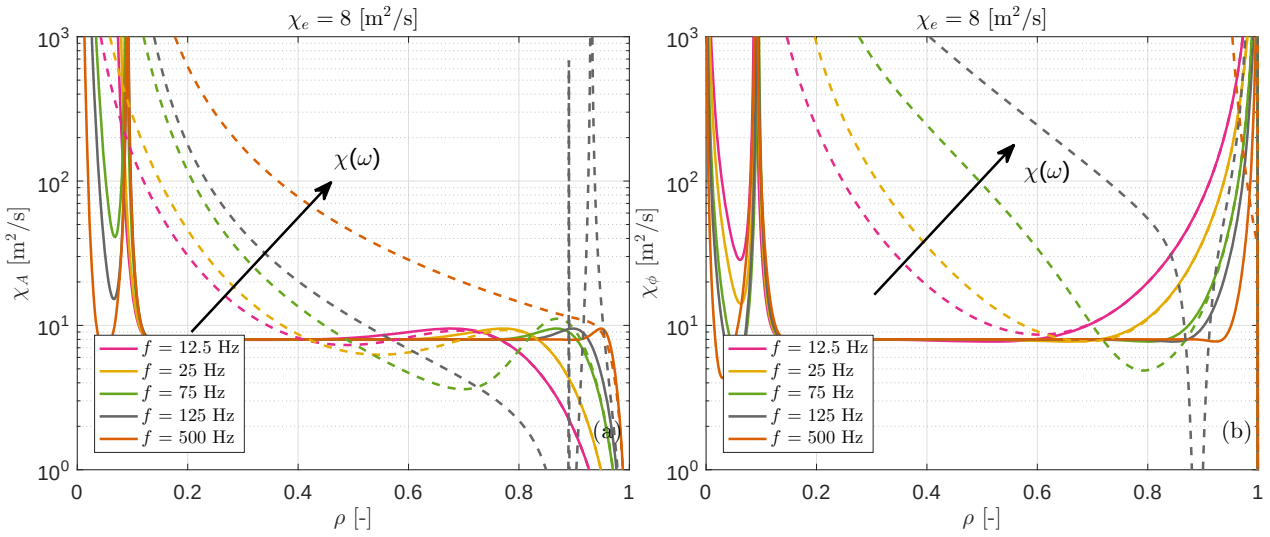

Figure 14. (a) The spatial dependency of the diffusion coefficient based on the temperature perturbations amplitude at different frequencies for a narrow deposition profile (lines) and wide redistributed profile (dashed-lines), which has been calculated using (23). (b) The spatial dependency of the diffusion coefficient based on the phase of temperature at different frequencies for a narrow deposition profile (lines) and wide redistributed profile (dashed-lines), which has been calculated using (23).

when analyzing high frequency modulation because when the frequency is increased the pulse becomes smaller and as (1) is an energy storage system also the size of the perturbation will become smaller, i.e., the amplitude of the perturbation decreases with frequency [45]. This has significant impact on the signal to noise ratio and in the case there is only a weak dependence on P it is questionable if this will still be visible. Moreover, as the mechanism for the redistribution is unknown, there is always the possibility that it has some frequency dependency. However, at the moment we do not have any evidence for the latter. Finally, we want to mention that in the linear context increasing amplitude does not change the physical transport coefficients and that linearity also implies that frequency components are independent.

6. Transport model and physical mechanisms

The previous sections show that based on experimental observations and empirical non-local models, transport can be split in a fast and slow time-scale. Moreover, it shows that for the fast time-scale either an error in the absorbed deposition occurs with respect to what is estimated or a fast transport mechanism is needed that spreads heat over a large radii. Combining these contributions in a linearized transport model results in a model presented in Fig. 15. It combines the different components affecting transport analyzed here. If the observed Lissajous curves are valid for all radii, then (2) gives an exact model for such measurements. The reason is that for all $\Delta\tilde{q}_e/n_e$ in Fig. 2 one can always find a $P_{eff}(\rho)$. Therefore, the next step is to fit experimental data onto this model and analyze how $P_{eff}(\rho)$ and $\chi(\rho)$ changes as function of various plasma parameters, which, we expect will give insight into the mechanisms explaining the measurements.

6.1. Discerning different transport components

The analysis in this paper shows that the slow and fast time-scale can be separated, which is summarized in Fig. 15. This is our first key step to understand this 30 year old problem. In case we use a symmetric block-wave (the standard) modulation: 1) The slopes can be used to estimate the diffusion coefficients; 2) The analysis in Sec. 3.2 shows that the height of the Lissajous curve $\Delta\tilde{q}_e/n_e$ can be used to estimate P_{eff}, which can be compared. In case we do not use a block-wave modulation or we have other slow transport components such as a convective velocity, more advanced methodologies are necessary. An example is the algorithm presented in [53], as the analysis in our paper shows if such methods are not applied the transport coefficients will be erroneous. In case of pure diffusive slow transport in Fig. 16 it is shown how to identify it from real experiments. Note that in high frequency modulation experiments the assumption that the slow time-scale of transport has little effect on the measurements still holds. As such one can use FFT to estimate the (effective) deposition profile or the break-in-slope method [54], which is shown in [54] to give similar results with respect to each other. However, as Fig. 13 (high frequency 500 Hz narrow vs. broad profile) and [21] shows in that case still P_{eff} is found and not necessarily the actual

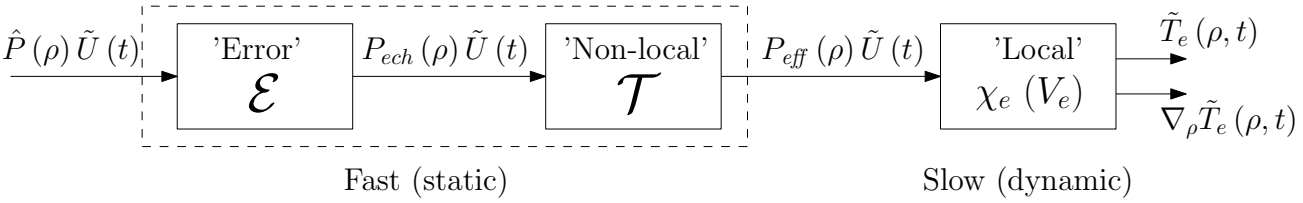

Figure 15. Transport model structure including the fast components and slow components including convective velocity V_e. This model should be able quantitatively reproduce experimental observations of Lissajous curves.

Table 1. Mechanisms which could be responsible for an apparent broadening of the deposition profile P_{eff}

$\mathcal{E}$ (heat deposition)	$\mathcal{T}$ (fast transport)
Deviation from Gaussian bundle (side-lobes)[46]	Turbulence broadening [47]
Multi-pass absorption [48]	Isotope effect [49]
Broadening due to edge turbulence [50]	MHD mode coupling [51, 6]
Thermal electrons [52]	

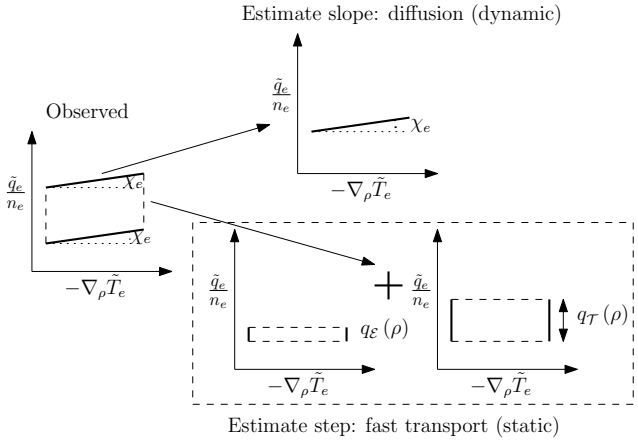

Figure 16. Overview of how to discern slow from fast transport, i.e., the combination from $\mathcal{E}$ and $\mathcal{T}$ in terms of their heat flux contributions $q_\mathcal{E}$ and $q_\mathcal{T}$ and the diffusive component χ_e. The combination of $q_\mathcal{E}$ and $q_\mathcal{T}$ can be re-expressed in terms of P_{eff}.

deposition profile.

Second key observation is that when the non-linear regime is entered then there is a relationship, see (19), between the slow time-scale and the fast time-scale according to local non-linear models $\chi(P)$. This means that at least it is theoretically possible to reconstruct part of $\mathcal{T}$. However, as P_{eff} has a significant impact on $\nabla_\rho T_e$ and T_e a change in P_{ech} can also affect the slow time-scale (critical gradients), which needs to be taken into account in the analysis.

Third important point is that $P_{eff}(\rho)$ should be independent of dependencies of the transport coefficients $\nabla_\rho T_e$ and T_e as they will only affect the slow time-scale. Hence, by identifying $P_{eff}(\rho)$, we can describe and predict how fast transport phenomena affect overall transport in fusion devices. The key will be to identify the structure of the combination of $\mathcal{E}$ and $\mathcal{T}$, which can range from a simple factor in case of non-absorbed heat, to complicated multi-dimensional non-linear kernel functions, if not more complicated. A key point of such experiments will be direct control over the total power without influencing the deposition profile, which is generally not the case when using multiple modulated ECRH-sources. This is difficult using old ECRH-systems. However, modern ECRH-systems, as available at W7-X [55], can do power modulation with various total power levels using a single source.

6.2. Physical mechanisms

Already for 30 years there is a debate on what causes the fast component on transport. A number of experiments have been performed to exclude certain physical mechanisms and discern the slow and fast time-scale. Especially, at W7-AS a lot of time was invested using various experiments to analyze the fast transport component. This includes high frequency modulation to remove the slow-scale transport from the ECE-measurements [4]. Also the effect of trapped electrons was investigated using a special magnetic hill configuration, which led to the conclusion that trapped electrons are not the cause of this observation [21]. These all show consistently that the power deposition profile from temperature measurements does not match the calculated deposition profiles using ray-tracing [3, 18], which are significantly narrower compared tot the profile from temperature measurements.

At LHD they did not perform such an analysis, but simply assumed that no error has been made in the calculation of the deposition profile [9, p. 4]. Moreover, the arguments are brought forward that as the spatial decay is non-monotonic (which can be reproduced using P_{eff}) and as a similar Lissajous curve is observed in the microscopic density fluctuations (turbulence level), it simply cannot be a deposition error [9]. In this paper it is shown that there must be

a redistribution of power P_{eff}, which is not localized around the deposition profile, but has a contribution over the entire plasma, based on phase delay between spatial locations, and the fact that the Lissajous curves show even for very large radii this behavior. In this paper, we do not analyze the mechanisms, but a non-exhaustive list of possible mechanisms which can cause a broadening of the deposition profile ($\mathcal{E}$) and transport mechanisms which can transport energy over distance on a fast time-scale ($\mathcal{T}$) is given in Table 1.

As we have not investigated which mechanism is responsible for the broadening, we can only speculate which mechanism is most likely to cause the broadening. In case of ECRH only the multi-pass absorption and especially broadening due to edge turbulence seem to be viable candidates as the other heating (loss) mechanisms are not expected to have a significant impact. For fast transport it is more difficult to attribute it to a specific mechanism.

7. Conclusion & Discussion

Based on the observations of linearity and observational studies of the direct dependence of transport on power in stellarators and tokamaks, we have shown that a linear model suffices to reproduce the Lissajous curves as presented in the literature. However, it is necessary to have an extra contribution to the heat flux which acts on a fast time-scale similar to that of the power modulation. We have shown that by analyzing the delay either a deposition profile that is much broader than predicted by ray-tracing codes or/and a fast (non-local) transport mechanism is necessary to explain the experimental observations. This showed that the absence of delay in experiments can only be explained if there is an effective heating term on all radii. Moreover, introducing such a term in the transport model allows a qualitative and in the future we will show a quantitative reproduction of the temperature profiles experimentally observed in stellarators. This additional term also fits exactly to the observations in various fusion machines with respect to the spatial amplitude and phase decay of the different harmonic components including tokamaks.

As the diffusive time-scale is much slower than that of the fast time-scale, it is possible to analyze these transport contributions separately. A fast time-scale related to heating and non-local contributions and a slow dynamic time-scale related to local parameters such as the diffusion and convective velocity.

In the future, five key issues need to be addressed:

(i) The observations on which this analysis is based are made in low-density plasmas in stellarators. Hence, a much larger class of discharges and machines need to be analyzed to see if this fast transport mechanism is also observed and what additional physics needs to be taken into account.

(ii) The estimation of the effective heating profile P_{eff} needs to be improved by using a direct estimation from temperature perturbations.

(iii) The standard estimation methods used in fusion to determine the diffusion coefficient fail under the influence of the additional fast transport component in the heat flux. Hence, the literature should carefully be reconsidered taking the possibility of such an estimation error in χ_e into account.

(iv) Statistical model validation techniques are necessary to verify if the heat flux model on which the estimate of χ_e is based is correct.

(v) Although perturbative experiments are largely linear in fusion devices, some non-linearities can be detected, which should be used to further investigate the non-linear component of the fast transport (mechanisms).

(vi) Finally, the correct mechanism or set of mechanisms need to be identified.

As has been discussed in Sec. 6, it is impossible to distinguish non-local transport and broadening of the deposition profile based on temperature measurements which are perturbed by small perturbations (linear) only. On the other hand, the non-local transport models show that over operating points there is a relationship between the slow and fast time-scale which only relates back to the non-local transport. For instance, the change in diffusion coefficient as function of power gives a contribution to both the slow and to the fast time-scale. The existence and specifically the quantification of this relationship using P_{eff} over different operating points should give independent non-linear models for non-local transport and deposition profile, e.g., changing the diffusion coefficient without changing the shape of the deposition profile. These measurement based models can be linearized again resulting in a deposition profile and a non-local transport contribution. Alternatively, P_{eff} can be studied varying deposition profiles and studying its correlation to ray-tracing, however, this is a more complicated approach. Both approaches are work in progress and if successful we will report on this in a new publication.

Acknowledgments

This work has been carried out within the framework of the EUROfusion Consortium and has received funding from the Euratom research and training programme 2014-2018 under grant agreement No 633053. The

views and opinions expressed herein do not necessarily reflect those of the European Commission.

Appendix A. Linearization

Assume a perturbation around an equilibrium

$$P\left(\rho,t\right)\approx P_0\left(\rho\right)+\tilde{P}\left(\rho,t\right), \tag{A.1}$$

which perturbs the temperature

$$T_e\left(\rho,t\right)\approx T_0\left(\rho\right)+\tilde{T}_e\left(\rho,t\right) \tag{A.2}$$

and the heat flux

$$q_e\left(\rho,t\right)\approx q_0\left(\rho\right)+\tilde{q}_e\left(\rho,t\right). \tag{A.3}$$

The heat equation in (1) is already linear, it can be restated in terms of perturbed quantities. The heat flux contributions of (12) need to be approximated by a Taylor expansion as follows

$$\begin{aligned} q_P\left(\rho,P\left(\rho,t\right)\right)&\approx q_P\left(\rho,P_0\left(\rho\right)\right)\\ &+\left(\left(\frac{\partial q_P}{\partial P}\left(\cdot,P_0\right)\right)\left(\tilde{P}\right)\right)\left(\rho,t\right)+h.o.t. \end{aligned} \tag{A.4}$$

and

$$\begin{aligned} \chi_e\left(\rho,P\left(\rho,t\right)\right)&\approx \chi_e\left(\rho,P_0\left(\rho\right)\right)\\ &+\left(\left(\frac{\partial \chi_e}{\partial P}\left(\cdot,P_0\right)\right)\left(\tilde{P}\right)\right)\left(\rho,t\right)+h.o.t. \end{aligned} \tag{A.5}$$

The notation $(\,)\left(\rho,t\right)$ is used to express that first the FrÃ©chet derivative needs to be taken and only then the equilibrium profiles should be substituted. The FrÃ©chet derivative is necessary as we do not know the dependence of q_P on P. To further clarify this, consider for example

$$q_P(\rho,P(\cdot,t))=\int_0^1 h(\rho,\xi)P(\xi,t)^2d\xi, \tag{A.6}$$

where $h\left(\rho,\xi\right)$ is some unknown kernel function. Then, the FrÃ©chet derivative can be analytically calculated as follows

$$\begin{aligned} &\left(\left(\frac{\partial q_P}{\partial P}\left(\cdot,P_0\right)\right)\left(\tilde{P}\right)\right)\left(\rho,t\right)=\\ &\qquad 2\int_0^1 h(\rho,\xi)P_0(\xi,t)\tilde{P}(\xi,t)d\xi. \end{aligned} \tag{A.7}$$

This dependency of q_P on ρ is still present at all radii. Let us continue with the linearization by substituting (A.4) and (A.5) in (12), i.e.,

$$\begin{aligned} &q_e\left(\rho,t\right)\approx\\ &\quad\underbrace{q_P\left(\rho,P_0\left(\rho\right)\right)-\chi_e\left(\rho,P_0\left(\rho\right)\right)n_e\nabla_\rho T_0\left(\rho\right)}_{\text{static } q_0(q_{offset})}\\ &\quad-\underbrace{\left(\frac{\partial \chi_e}{\partial P}\left(\cdot,P_0\right)\right)\left(\tilde{P}\right)\left(\rho,t\right)n_e\nabla_\rho\tilde{T}_e\left(\rho,t\right)}_{\text{product of perturbations, i.e., negligible}}\\ &\quad+\left(\left(\frac{\partial q_P}{\partial P}\left(\cdot,P_0\right)\right)\left(\tilde{P}\right)\right)\left(\rho,t\right)\\ &\quad-\left(\frac{\partial \chi_e}{\partial P}\left(\cdot,P_0\right)\right)\left(\tilde{P}\right)\left(\rho,t\right)n_e\nabla_\rho T_0\left(\rho\right)\\ &\quad-\chi_e\left(\rho,P_0\left(\rho\right)\right)n_e\nabla_\rho\tilde{T}_e\left(\rho,t\right), \end{aligned} \tag{A.8}$$

such that only the last three terms need to be considered in $\tilde{q}_e$. This results for $\tilde{q}_e\left(\rho,t\right)$ in (14).

Appendix B. Calculation of the time delay of $\nabla_\rho T_e$ in a source-less slab-geometry semi-infinite half-space

The partial differential equation in (4) can be simplified by assuming pure diffusion with constant density on a slab domain (approximation of cylindrical domain at large radii) without heating. This results in the simplification

$$\frac{\partial\tilde{T}_e\left(\rho,t\right)}{\partial t}\qquad=\qquad\frac{\partial}{\partial\rho}\left(\chi_e\frac{\partial\tilde{T}_e\left(\rho,t\right)}{\partial\rho}\right). \tag{B.1}$$

Transforming this into the frequency domain results in

$$i\omega\Theta\left(\rho,\omega\right)=\frac{\partial}{\partial\rho}\left(\chi_e\frac{\partial\Theta\left(\rho,\omega\right)}{\partial\rho}\right),$$

where $\Theta\left(\omega,\rho\right)$ is the Fourier transform of the temperature, i.e., $\Theta\left(\rho,\omega\right)=\mathcal{F}\left(\tilde{T}_e\left(\rho,t\right)\right)$. The solution for a semi-infinite domain, i.e., for $\rho\rightarrow\infty$,$\Theta\left(\rho,\omega\right)=0$, and boundary condition $\Theta\left(\rho_1,\omega\right)=\Theta\left(\rho_1,\omega\right)$ results in following solution

$$\Theta\left(\omega,\rho\right)=\exp\left(-\sqrt{\frac{i\omega}{\chi_e}}\left(\rho-\rho_1\right)\right)\Theta\left(\rho_1,\omega\right), \tag{B.2}$$

which is also given in [40, 41]. The ratio (transfer function) between the temperature at location ρ_1, $\Theta\left(\rho_1,\omega\right)$, and at an arbitrary location ρ, $\Theta\left(\omega,\rho\right)$, is generally used to determine the temperature perturbation. Its spatial derivative is given by

$$\frac{\partial\Theta\left(\rho,\omega\right)}{\partial\rho}=-\sqrt{\frac{i\omega}{\chi_e}}\exp\left(-\sqrt{\frac{i\omega}{\chi_e}}\left(\rho-\rho_1\right)\right)\Theta\left(\rho_1,\omega\right). \tag{B.3}$$

Rewriting (B.3) in terms of $A\exp(i\phi)$ yields

$$\frac{\partial\Theta(\rho,\omega)}{\partial\rho} = -\sqrt{\frac{\omega}{\chi_e}}\exp\left(-\sqrt{\frac{\omega}{2\chi_e}}(\rho-\rho_1)\right) \exp\left(\left(-\sqrt{\frac{\omega}{2\chi_e}}(\rho-\rho_1)+\frac{\pi}{4}\right)i\right)\Theta(\rho_1,\omega), \quad \text{(B.4)}$$

such that the relative delay $\Delta\tau$ [s] of $\nabla_\rho T_e$ is given by

$$\Delta\tau = -\frac{1}{\omega}\left(\sqrt{\frac{\omega}{2\chi_e}}(\rho-\rho_1)-\frac{\pi}{4}\right), \quad \text{(B.5)}$$

when χ_e is dimensionless. In case χ_e has dimension $[m^2/\text{s}]$, $\rho-\rho_1$ should be multiplied with a. This equation can be used to calculate the delay for a specific frequency from one location to another assuming no heating on the domain $[\rho_1,\rho]$. As here the delay is described in terms of a phase delay, the minus sign can also be omitted.

Now, consider ρ_1 to be the deposition location ρ_{dep} and assuming no heating on the slab geometry semi-infinite domain except at the deposition location itself ρ_{dep}. Then $\Delta\tau$ depends on three factors: the frequency, the transport coefficients, here diffusion only, and the distance to the center of deposition. Note that this delay should not be interpreted as dead-time, but as the phase difference in terms of seconds. The reason is that mathematically the response to a perturbation in (1) is always instant, but effectively it takes some time to see the actual response.

The frequency used in the experiment was 25 Hz. Hence, the delay as function of $\Delta\rho=\rho-\rho_{dep}$ becomes

$$\Delta\tau = 20\cdot\Delta\rho\cdot a - 5\,[\text{ms}]$$

and consequently a delay of $\Delta\tau = 17$ [ms] will occur for a distance of $\Delta\rho = 0.5$ in slab geometry.

References

[1] TFR Group and FOM ECRH Team 1988 *Nucl. Fusion* **28** 1995

[2] Fredrickson E D, McGuire K, Cavallo A, Budny R, Janos A *et al.* 1990 *Phys. Rev. Lett.* **65** 2869–2872

[3] Hirsch M, Baldzuhn J, Beidler C, Brakel R, Burhenn R, Dinklage A *et al.* 2008 *Plasma Phys. Control. Fusion* **50** 053001

[4] Hartfuss H J, Endler M, Erckmann V, Gasparino U, Giannone L *et al.* 1994 *Plasma Phys. Control. Fusion* **36** B17

[5] Stroth U 1998 *Plasma Phys. Control. Fusion* **40** 9

[6] Pustovitov V D 2012 *Plasma Phys. Control. Fusion* **54** 124036

[7] Rodriguez-Fernandez P, White A E, Howard N T, Grierson B A, Staebler G M, Rice J E *et al.* 2018 *Phys. Rev. Lett.* **120**(7) 075001

[8] Peters M 1996 *Electron heat transport in current carrying and currentless thermonuclear plasmas : tokamaks and stellarators compared* Phd thesis URL `https://pure-tue-nl.dianus.libr.tue.nl/ws/files/1550470/452099.pdf`

[9] Inagaki S, Tokuzawa T, Tamura N, Itoh S I, Kobayashi T, Ida K, Shimozuma T, Kubo S, Tanaka K, Ido T *et al.* 2013 *Nucl. Fusion* **53** 113006

[10] van Berkel M, Kobayashi T, Igami H, Vandersteen G, Hogeweij G M D, Tanaka K, Tamura N, de Baar M R, Zwart H J, Kubo S, Ito S, Tsuchiya H and the LHD Experiment Group 2017 **57**

[11] Hartfuss H J, Giannone L, Stroth U, Erckmann V, Gasparino U, Maassberg H, W7-AS-team and ECRH-team 1994 Heat wave studies on W7-AS stellarator *Proceedings of the workshop on 'Local Transport Studies in Fusion', Varenna 1993* pp 119 – 125

[12] Lopes Cardozo N J 1995 *Plasma Phys. Control. Fusion* **37** 799

[13] Jacchia A, Mantica P, De Luca F, Galli P and Gorini G 1995 *Phys. Plasmas* **2** 4589–4595

[14] del Castillo-Negrete D 2006 *Phys. Plasmas* **13** 082308

[15] del Castillo-Negrete D, Mantica P, Naulin V, Rasmussen J and JET-EFDA contributors 2008 *Nucl. Fusion* **48** 075009

[16] Garbet X, Sarazin Y, Imbeaux F, Ghendrih P, Bourdelle C, Gürcan Ã D and Diamond Ã D 2007 *Phys. Plasmas* **14** 122305

[17] Mantica P and Ryter F 2006 *C. R. Phys.* **7** 634–649

[18] Kirov K K, Leuterer F, Pereverzev G V, Ryter F, Suttrop W and ASDEX Upgrade team 2002 *Plasma Phys. Control. Fusion* **44** 2583

[19] Romé M, Erckmann V, Gasparino U, Hartfuss H J, Kühner G, Maassberg H and Marushchenko N 1997 *Plasma Phys. Control. Fusion* **39** 117

[20] Lawrence J 1972 *A catalog of special plane curves* (Dover Publications, NY)

[21] Stroth U, Giannone L, Hartfuss H J, ECH Group and the W7-AS Team 1996 *Plasma Phys. Control. Fusion* **38** 611

[22] Khalil H K 1996 *Noninear Systems* (Prentice-Hall (NJ))

[23] van Berkel M, Zwart H, Hogeweij G and de Baar M 2017 *Plasma Phys. Control. Fusion* **59** 062001

[24] Stroth U, Branas B, Estrada T, Giannone L, Hartfuss H J *et al.* 1995 *Physica Scripta* **51** 655 URL `http://stacks.iop.org/1402-4896/51/i=5/a=019`

[25] Heath M 1997 *Scientific computing* (McGraw-Hill, New York (NY))

[26] Itoh S I and Itoh K 2013 *Nucl. Fusion* **53** 073035

[27] Itoh K *et al.* 2016 *J. Phys. Soc. Jpn* **85** 014501

[28] Itoh S I, Inagaki S, Dong J and Itoh K 2016 *Plasma and Fusion Research: Overview Articles*

[29] Yamazaki K and Amano T 1992 *Nucl. Fusion* **32** 633

[30] Vargas V, Lopez-Bruna D, Herranz J, Castejon F and the TJ-II Team 2007 *Nucl. Fusion* **47** 1367

[31] Vargas V I, López-Bruna D, García J, Fernández A, Cappa A, Herranz J, Castejón F and Melnikov A 2008 ECH power dependence of electron heat diffusion in ECH plasmas of the TJ-II stellarator *35th EPS Conf. Plasma Physics* vol 32

[32] van Berkel M, Kobayashi T, Vandersteen G, Zwart H J, Igami H, Kubo S *et al.* 2018 *submitted to Nucl. Fusion*

[33] Mantica P, Peters M, De Luca F, De Lauri A, Gorini G, Hogeweij G, Jacchia A and Lopes Cardozo N 1996 *Nucl. Fusion* **36** 1317 URL `http://stacks.iop.org/0029-5515/36/i=10/a=I05`

[34] Curtain R F and Zwart H J 1995 *An Introduction to Infinite-Dimensional Linear Systems Theory* vol 21 (Springer-Verlag, Berlin-Heidelberg)

[35] Gentle K W 1988 *Phys. Fluids B-Plasma* **31** 1105

[36] Ryter F, Angioni C, Beurskens M, Cirant S, Hoang G T, Hogeweij G M D *et al.* 2001 *Plasma Phys. Control. Fusion* **43** A323 URL `http://stacks.iop.org/0741-3335/43/i=12A/a=325`

[37] Imbeaux F, Ryter F and Garbet X 2001 *Plasma Phys. Control. Fusion* **43** 1503

[38] Ryter F, Angioni C, Peeters A G, Leuterer F, Fahrbach H U and Suttrop W (ASDEX Upgrade Team) 2005 *Phys. Rev. Lett.* **95**(8) 085001
[39] Mantica P, Strintzi D, Tala T, Giroud C, Johnson T, Leggate H, Lerche E, Loarer T, Peeters A G, Salmi A *et al.* 2009 *Phys. Rev. Lett.* **102** 175002
[40] Jacchia A, Mantica P, De Luca F and Gorini G 1991 *Phys. Fluids B-Plasma* **3** 3033–3040
[41] van Berkel M, Zwart H J, Tamura N, Hogeweij G M D, Inagaki S, de Baar M R and Ida K 2014 *Phys. Plasmas* **21** 112507
[42] van Berkel M, Zwart H J, Hogeweij G M D, Vandersteen G, van den Brand H, de Baar M R and the ASDEX Upgrade Team 2014 *Plasma Phys. Control. Fusion* **56** 105004.
[43] Kobayashi T, Ida K, Inagaki S, Moon C, Tsuchiya H, van Berkel M, Choe G H *et al.* 2016 Analysis of higher harmonics on bi-directional heat pulse propagation experiment in helical and tokamak devices *IAEA Conference*
[44] Inagaki S, Itoh S I, Itoh K, Kasuya N, Kobayashi T *et al.* 2013 *Plasma and Fusion Research* **8** 1202173–1202173
[45] van Berkel M, de Cock A, Hogeweij G M D, Vandersteen G, Zwart H J and de Baar M R 2018 *Phys. plasmas (under minor revisions)*
[46] Tsironis C, Poli E and Pereverzev G V 2006 *Physics of plasmas* **13** 113304
[47] Hahm T S, Diamond P, Lin Z, Itoh K and Itoh S 2004 *Plasma Phys. Control. Fusion* **46** A323
[48] Lloyd B 1998 *Plasma physics and controlled fusion* **40** A119
[49] Itoh S and Itoh K 2018 *Plasma Physics and Controlled Fusion* **60** 035008
[50] Thomas M B, Brookman M W, Austin M E, Köhn A, La Haye R J, Leddy J B, Vann R G and Yan Z 2017 *arXiv preprint arXiv:1710.03028*
[51] van Milligen B P, Nicolau J H, Garcia L, Carreras B A, Hidalgo C and the TJ-II Team 2017 *Nuclear Fusion* **57** 056028 URL `http://stacks.iop.org/0029-5515/57/i=5/a=056028`
[52] Coda S, Alberti S, Blanchard P, Goodman T P, Henderson M A, Nikkola P, Peysson Y and Sauter O 2003 *Nucl. Fusion* **43** 1361
[53] Eguilior S, Castejón F, de la Luna E, Cappa A, Likin K, Fernández A and TJ-II Team 2003 *Plasma Phys. Control. Fusion* **45** 105
[54] Lerche E, Van Eester D *et al.* 2008 *Plasma Physics and Controlled Fusion* **50** 035003
[55] Erckmann V, Brand P, Braune H, Dammertz G, Gantenbein G, Kasparek W, Laqua H, Maassberg H, Marushchenko N, Michel G *et al.* 2007 *Fusion Science and Technology* **52** 291–312